frontiers in Physics

ORIGINAL RESEARCH
published: 20 May 2020
doi: 10.3389/fphy.2020.00141

Terahertz Switch Utilizing Inorganic Perovskite-Embedded Metasurface

Ri-Hui Xiong[1], *Xiao-Qing Peng*[2] *and Jiu-Sheng Li*[1]*

[1] Centre for THz Research, China Jiliang University, Hangzhou, China, [2] State Grid Sichuan Electric Power Company, Chengdu, China

Various applications of terahertz technology require a large number of various terahertz wave control devices. Yet, high efficient and rapid-response terahertz switch is still a great challenge. Here, we introduce a new scheme, based on inorganic perovskite quantum dot ($CsPbBr_3$-QD)-embedded metasurface under different pump laser powers that realize terahertz wave high-speed switching performance. The off–on speed of the presented device achieves 8 MHz. This kind of components provides a new idea and a cost-effective functional solution for manipulating the terahertz waves in emerging terahertz devices and systems.

Keywords: terahertz wave switch, metasurface, switching speed, terahertz, inorganic pervoskite

OPEN ACCESS

Edited by:
Lin Chen,
University of Shanghai for Science and Technology, China

Reviewed by:
Fei Fan,
Nankai University, China
Rajour Tanyi Ako,
RMIT University, Australia

***Correspondence:**
Jiu-Sheng Li
lijsh2008@126.com

Specialty section:
This article was submitted to Optics and Photonics, a section of the journal Frontiers in Physics

Received: *22 January 2020*
Accepted: *09 April 2020*
Published: *20 May 2020*

Citation:
Xiong R-H, Peng X-Q and Li J-S (2020) Terahertz Switch Utilizing Inorganic Perovskite-Embedded Metasurface. Front. Phys. 8:141. doi: 10.3389/fphy.2020.00141

INTRODUCTION

Terahertz technology shows great promise for many applications including sensing, spectroscopy, non-destructive imaging, security monitoring, and wireless communications [1–4]. In particular, wireless communication using terahertz wave has attracted much interest due to large frequency bandwidth and high data transmission speed [5, 6]. These applications require the ability to flexibly manipulate terahertz wave in free space. Over the past several years, many kinds of terahertz wave devices have been reported such as filter [7], polarizer [8], power divider [9], modulator [10], absorber [11], switch [12], etc. As the core device of terahertz wave system, terahertz wave switch has received significant attention. Several techniques have been introduced to implement terahertz wave switch by applying external magnetism, electricity, temperature, and light illumination stimuli [13–17]. However, manipulating terahertz wave to achieve high efficient and rapid switching performance in a device is a great challenge.

Inorganic perovskite quantum dots ($CsPbBr_3$-QDs) have recently gained significant attention in photovoltaic applications demonstrating power conversion efficiencies in solar cells, high charge-carrier mobility [18, 19], and longer diffusion lengths [20]. Under the excitation of optical pump fluences, the perovskite exhibits high light absorption and short carrier recombination lifetime on nanosecond [21, 22]. Using these properties of perovskite, they are combined with subwavelength metasurface structures, and their properties can be enhanced or exploited as an efficient terahertz manipulation device. In this work, we described a method for the active control of terahertz wave transmission using $CsPbBr_3$-QD-embedded metasurface. By using commercially available finite difference frequency domain solver CST Microwave Studio, we obtained the optimized dimensions of the $CsPbBr_3$-QD-embedded metasurface. Finally, we experimentally demonstrate the switching phenomenon in the $CsPbBr_3$-QD embedded metasurface using optical stimuli. The proposed switch approach will be of great significance for practical terahertz applications.

DESIGN AND ANALYSIS

Figure 1A illustrates the configuration of the $CsPbBr_3$-QD-embedded metasurface-based terahertz wave switch. The top layer employs the inorganic perovskite QD-embedded metasurface as the geometric cell, and it is printed on a silicon oxide (100 nm)/high resistance silicon dielectric substrate with relative permittivity of $\varepsilon_{si} = 11.9$ and a thickness of 200 μm. The metasurface is made of copper with a conductivity of 5.96×10^7 m/s and a thickness of 300 nm. The dielectric constant of copper from 0.2 THz to 1.0 THz is $\varepsilon_{cu} = -7.479 \times 10^4 + i2.723 \times 10^6 \sim -7.345 \times 10^4 + i5.338 \times 10^5$. The dielectric constant of inorganic perovskite QD perovskite in the frequency band 0.2∼1.0 THz is $\varepsilon_p = 9.2$ without laser irradiation [17]. The period of the unit cell is 100 μm. Optical microscope image of the fabricated $CsPbBr_3$-QD-embedded metasurface is shown in **Figure 1B**. We use the Drude model to describe the perovskite complex conductivity, which can be expressed by Yettapu et al. [22].

$$\delta(\omega) = \frac{\varepsilon_0 \omega_p^2}{t_\Gamma - i\omega}\left(1 + \frac{Ct_\Gamma}{t_\Gamma - i\omega}\right) \quad (1)$$

where $\omega_p = \sqrt{n}e^2/\varepsilon_0 m$ is the plasma frequency, t_Γ is the carrier scattering rate as $t_\Gamma = e/m^*v$, m^* is the carrier effective mass, $m = 0.5(m_e + m_h)$, $m_e = 0.22$, and $m_h = 0.24$. The C parameter, which represents the degree of carrier localization, may have values between 0 and −1. Without laser irradiate, we can choose $C = 0$. While with laser irradiate, we set $C = -1$. The relationship between the conductivity of perovskite and pump laser radiation can be obtained in Chanana et al. [23].

A commercially available finite difference frequency domain solver software CST Microwave Studio was used to simulate the metasurface structure. We use an adaptive mesh with a size of λ/10, where λ is the wavelength of incident radiation. The surrounding boundary condition was set as the periodic boundary, and an open boundary condition is set along the direction of the terahertz wave propagation. **Figure 2** shows the terahertz transmission spectra of the different parts of our proposed metasurface unit cell. One can see that only the $CsPbBr_3$-QD-embedded metasurface unit cell achieved narrow band resonance effects for enhancing the interaction between the terahertz wave and the metasurface. We also numerically analyze the terahertz transmission properties of the structure with different size parameters *g*, *s*, *d*, and *a*. In **Figure 3**, we can find that these parameters only have a weak influence on the position and width of transmission peak at 0.6 THz. After completing the optimization process, the geometrical dimensions of the geometric pattern metasurface have been set as follows: $a = 75$ μm, $g = 12$ μm, $s = 12$ μm, and $d = 70$ μm.

DEVICE FABRICATION

The metasurface was fabricated using the conventional photolithography technique. First, positive photoresist was coated on a silicon substrate and prebaked at 105°C for 1 min. Then, the mask was aligned and exposed under UV-light. The sample was immersed in the developer solution to remove the exposed part of the photoresist. A 300-nm-thick copper was deposited by thermal evaporation, and the sample was removed in acetone solution to obtain the designed metal pattern. Second, a thin layer of parylene c was deposited by vapor deposition to make the parylene film completely cover the sample, followed by a certain complementary pattern in the photoresist. The parylene film was etched with oxygen plasma, leaving a through hole, in which $CsPbBr_3$ perovskite QDs can be deposited. After solution casting and annealing of the desired $CsPbBr_3$ perovskite QD film, once the $CsPbBr_3$ perovskite QD film starts to crystallize, usually after 60 s, the parylene film will be layered. Finally, the samples were thoroughly annealed to obtain a high-quality polycrystalline pattern structure.

RESULTS AND DISCUSSION

A terahertz time domain spectroscopy (THz-TDS) system was used to measure the transmission spectra of the sample

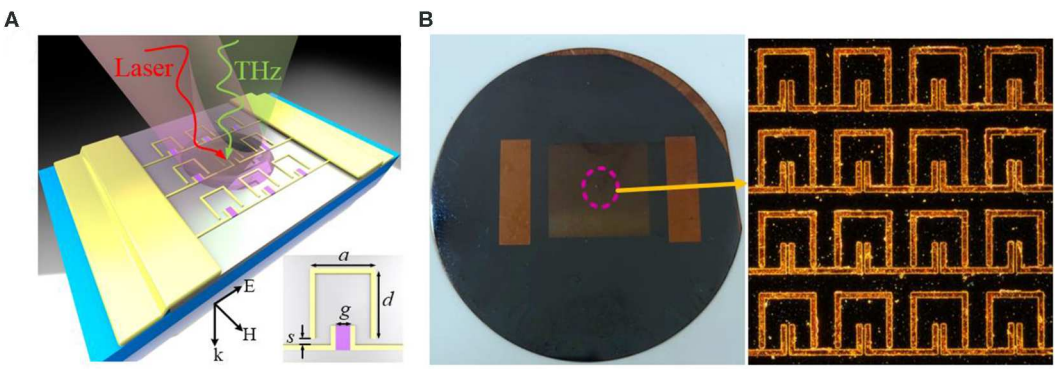

FIGURE 1 | (A) Three-dimensional schematic diagram of the proposed metasurface embedded with perovskite quantum dots ($CsPbBr_3$-QDs). **(B)** Optical microscope image of the fabricated $CsPbBr_3$-QD-embedded metasurface (geometric parameters of the metasurface unit cell, $a = 75$ μm, $g = 12$ μm, $s = 12$ μm, and $d = 70$ μm).

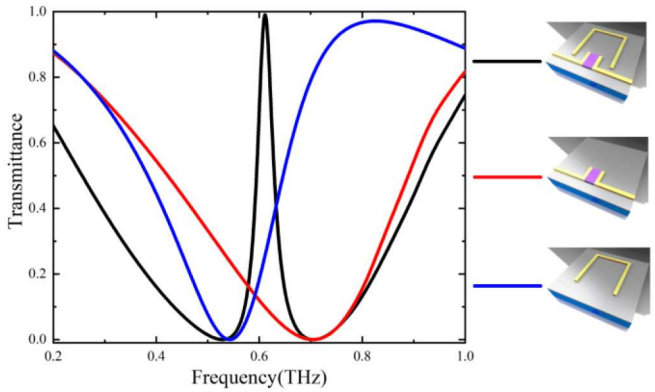

FIGURE 2 | Terahertz transmission spectra of the different parts of the proposed metasurface unit cell.

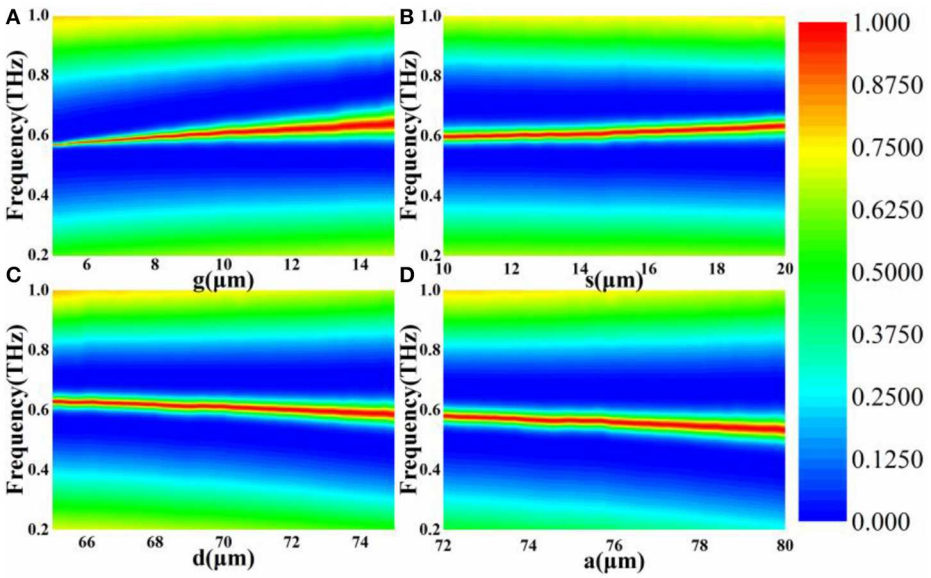

FIGURE 3 | Terahertz transmittance contour plot for various geometrical parameters values of our proposed $CsPbBr_3$-QD-embedded metasurface **(A)** *g*, **(B)** *s*, **(C)** *d*, **(D)** *a*.

with a different power density. The excitation source was a Ti:sapphire laser with 100-fs duration at 80-MHz repetition rate, and working wavelength at 780 nm. Terahertz pulse was generated using LT-GaAs photoconductive antenna, and a ZnTe nonlinear crystal was used to detect the terahertz signal. The $CsPbBr_3$-QD-embedded metasurfaces were placed at the confocal position of the system. The entire experiment was carried out in nitrogen environment. The recorded terahertz transmission time domain spectra are shown in **Figure 4A**, for varying the CW pumping laser fluence. **Figure 4B** shows the terahertz frequency domain spectra by Fourier transformation from the time domain data under various laser pump powers. In **Figure 4**, one can see that the transmission spectra of the $CsPbBr_3$-QD-embedded metasurface declines gradually as the pumping laser power increases. When the pumping power increases to 240 $\mu J/cm^2$, the transmittances of the terahertz wave drops to 10.9% at 0.5 THz. It indicates that the sample can control the terahertz wave transmission under a different pump laser power.

The terahertz transmission switching performance of our proposed structure was investigated in terahertz continuous wave system (see **Figure 5**). **Figure 6** plots the measured dynamic characteristics of the proposed $CsPbBr_3$-QD-embedded metasurface structure with various laser pump fluences. **Figures 6A,B** illustrate the detected voltage signal waveform shape for switching speeds of 10 KHz and 8 MHz. One can see that the transmission amplitude of terahertz wave decreases with the switching speed increase from 10 KHz to 8 MHz.

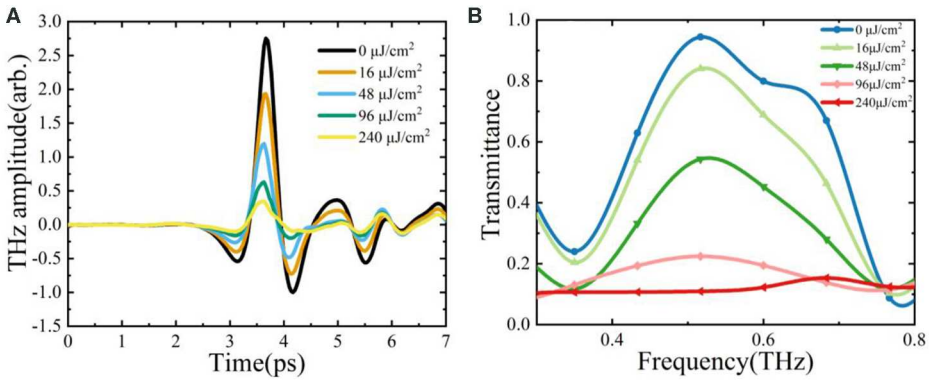

FIGURE 4 | (A) Measured terahertz transmission time domain spectra using the terahertz time domain spectroscopy (THz-TDS) under a different laser power. **(B)** Corresponding terahertz frequency domain spectra.

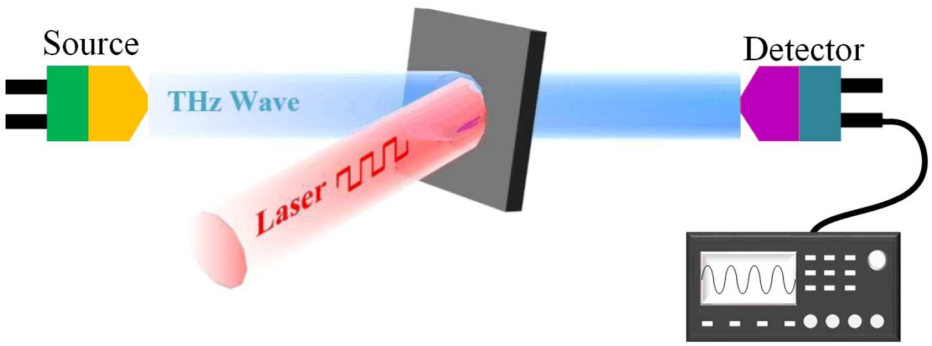

FIGURE 5 | Dynamic switching measurement using a backward-wave oscillator (BWO) CW terahertz source and Schottky diode detector.

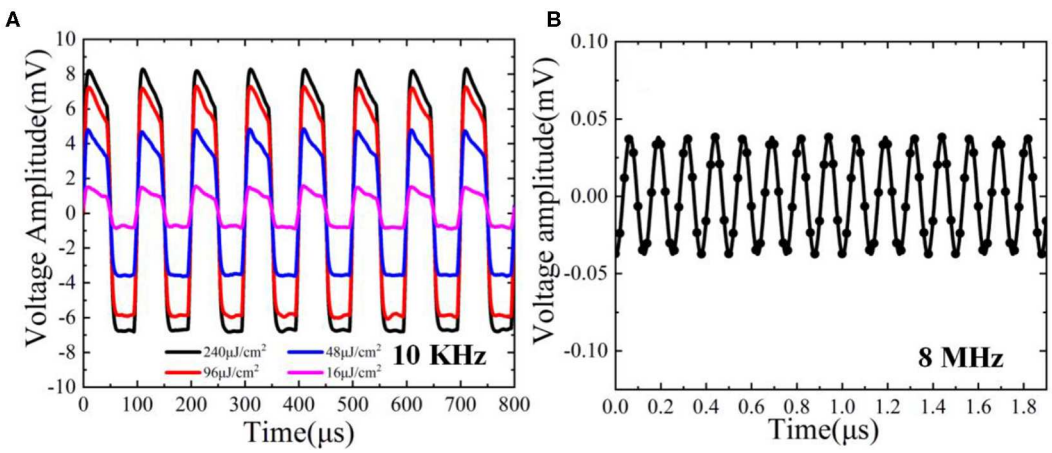

FIGURE 6 | (A) A 10-KHz switching speed under different pump laser fluencies. **(B)** An 8-MHz switching speed of the sample.

At switching speed of 8 MHz, the detected voltage amplitude falls to 0.05 mV. **Figure 7A** shows the terahertz transmission intensity distribution through the $CsPbBr_3$-QD-embedded metasurface structure without pump laser fluence. The terahertz wave transmission intensity drops to 10.9% of its original value under 240 $\mu J/cm^2$ pump laser intensity. As depicted in **Figure 7B**, the corresponding extinction ratio is 83%. **Figure 7C** shows the extinction ratio dependence of the pump laser fluence

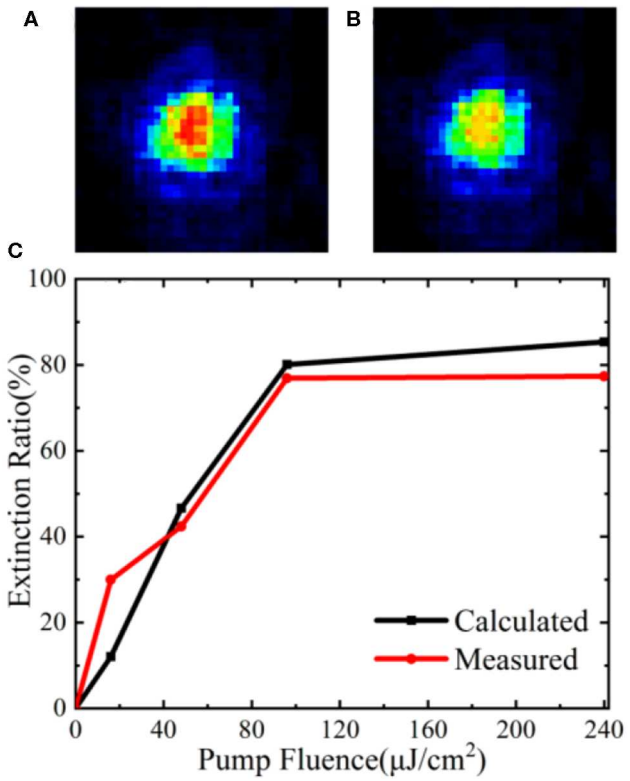

FIGURE 7 | Terahertz intensity distributions through the $CsPbBr_3$-QD-embedded metasurface. **(A)** 0 $\mu J/cm^2$ and **(B)** 240 $\mu J/cm^2$ pump laser intensity. **(C)** Extinction ratio dependence of pump laser intensity.

obtained by experiment and calculation. One sees that the $CsPbBr_3$-QD-embedded metasurface has low saturation pump laser intensity and high extinction ratio factor as a potential method to actively control the terahertz wave transmission. This work demonstrates a new approach for realizing active terahertz devices with improved functionalities.

CONCLUSION

We describe a method for the active control of terahertz wave transmission using $CsPbBr_3$-QD-embedded metasurface. The experimental results confirm the numerically simulated expectations. With the external applied pump laser irradiation, our presented terahertz device achieves high-efficiency terahertz wave switch with an off–on speed of 8 MHz. Owing to effective switching and easy fabrication, this device has promising applications as a controllable switch in future terahertz wave communication and imaging systems.

DATA AVAILABILITY STATEMENT

All datasets generated for this study are included in the article/supplementary material.

AUTHOR CONTRIBUTIONS

R-HX performed the THz measurements and did the calculations. X-QP fabricated and characterized the devices. J-SL concerned the devices structure and developed the theoretical model and guided the experimental work. All authors discussed the results and co-wrote the manuscript.

ACKNOWLEDGMENTS

The authors acknowledge valuable discussion on experiment with Dr. J. Liu. This work was sponsored by the National Natural Science Foundation of China (61871355, 61831012) and Zhejiang Lab (NO.2019LC0AB03).

REFERENCES

1. Chan W, Deibel J, Mittleman D. Imaging with terahertz radiation. *Report Progr Phys.* (2007) **70**:1325. doi: 10.1088/0034-4885/70/8/R02
2. Koenig S. Wireless sub-THz communication system with high data rate. *Nat Photon.* (2013) **7**:977. doi: 10.1038/nphoton.2013.275
3. Han P, Cho G, Zhang X. Time-domain transillumination of biological tissues with terahertz pulses. *Opt Lett.* (2000) **25**:242. doi: 10.1364/OL.25.000242
4. Savo S, Shrekenhamer D, Padilla W. Liquid crystal metamaterial absorber spatial light modulator for THz applications. *Adv Opt Mater.* (2014) **2**:275–9. doi: 10.1002/adom.201300384
5. Wang J, Tian H, Wang Y, Li X, Cao Y, Li L, et al. Liquid crystal terahertz modulator with plasmon-induced transparency metamaterial. *Opt Exp.* (2018) **26**:5769–76. doi: 10.1364/OE.26.005769
6. Sensale-Rodriguez B, Yan R, Kelly M. Broadband graphene terahertz modulators enabled by intraband transitions. *Nat Commun.* (2012) **3**:780. doi: 10.1038/ncomms1787
7. Tabatabaei F, Biabanifard M, Abrishamian M. Terahertz polarization-insensitive and all-optical tunable filter using Kerr effect in graphene disks arrays. *Optik.* (2019) **180**:526 doi: 10.1016/j.ijleo.2018.11.103
8. Yu T, Chi N, Tsai H, Wang S, Luo C, Chen K. Robust terahertz polarizers with high transmittance at selected frequencies through Si wafer bonding technologies. *Opt Lett.* (2017) **42**:4917 doi: 10.1364/OL.42.004917
9. Reichel K, Mendis R, Mittleman D. A broadband terahertz waveguide T-junction variable power splitter. *Sci Rep.* (2016) **6**:28925 doi: 10.1038/srep28925
10. Hochberg M, Baehrjones T, Wang G, Shearn M, Harvard K, Luo J. Terahertz all-optical modulation in a silicon-polymer hybrid system. *Nat Mater.* (2006) **5**:703–9 doi: 10.1038/nmat1719
11. Grant J, Ma Y, Saha S, Lok L, Khalid A, Cumming D. Polarization insensitive, broadband terahertz metamaterial absorber. *Opt Lett.* (2011) **36**:3476–8 doi: 10.1364/OL.36.003476
12. Kupchak C, Erskine J, England D, Sussman B. Terahertz-bandwidth switching of heralded single photons. *Opt Lett.* (2019) **44**:1427 doi: 10.1364/OL.44.001427
13. Li J, He J, Hong Z. Terahertz wave switch based on silicon photonic crystals. *Appl Opt.* (2007) **46**:5034–7. doi: 10.1364/AO.46.005034
14. Chen S, Fan F, Miao Y, He X, Zhang K, Chang S. Ultrasensitive terahertz modulation by silicon-grown MoS_2 nanosheets. *Nanoscale.* (2016) **8**:4713–9. doi: 10.1039/C5NR08101G

15. Zheng W, Fan F, Chen M, Chen S, Chang S. Optically pumped terahertz wave modulation in MoS_2-Si heterostructure metasurface. *AIP Adv.* (2016) **6**:075105. doi: 10.1063/1.4958878
16. Liu W, Fan F, Xu S, Chen M, Wang X, Chang S. Terahertz wave modulation enhanced by laser processed PVA film on Si substrate. *Sci Rep.* (2018) **8**:8304. doi: 10.1038/s41598-018-26778-7
17. Luo L, Wang K, Ge C, Guo K, Shen F, Yin Z, et al. Actively controllable terahertz switches with graphene-based nongroove gratings. *Photonics Res.* (2017) **5**:604. doi: 10.1364/PRJ.5.000604
18. Snaith H. Perovskites: the emergence of a new era for low-cost, high-efficiency solar cells. *J Phys Chem Lett.* (2013) **4**:3623–30. doi: 10.1021/jz4020162
19. Green M, Ho-Baillie A, Snaith H. The emergence of perovskite solar cells. *Nat Photon.* (2014) **8**:506–14. doi: 10.1038/nphoton.2014.134
20. Stranks S, Eperon G, Grancini G, Menelaou C, Alcocer M, Leijtens T, et al. Electron-hole diffusion lengths exceeding 1 micrometer in an organometal trihalide perovskite absorber. *Science.* (2013) **342**:341–4. doi: 10.1126/science.1243982
21. Herz L. Charge-carrier dynamics in organic-inorganic metal halide perovskites. *Annu Rev Phys Chem.* (2016) **67**:65–89. doi: 10.1146/annurev-physchem-040215-112222
22. Yettapu G, Talukdar D, Sarkar S, Swarnkar A, Nag A, Ghosh P. THz conductivity within colloidal $CsPbBr_3$ perovskite nanocrystals: remarkably high carrier mobilities and large diffusion lengths. *Nano Lett.* (2016) **16**:4838. doi: 10.1021/acs.nanolett.6b01168
23. Chanana A, Liu X, Zhang C, Vardeny Z, Nahata A. Ultrafast frequency-agile terahertz devices using methylammonium lead halide perovskites. *Sci Adv.* (2018) **4**:7353. doi: 10.1146/annurev-physchem-040215-112222

Conflict of Interest: The authors declare that the research was conducted in the absence of any commercial or financial relationships that could be construed as a potential conflict of interest.